*Robotica* (2024), **42**, pp. 2635–2657
doi:10.1017/S0263574724000997

CAMBRIDGE UNIVERSITY PRESS

RESEARCH ARTICLE

# Adaptive integral terminal sliding mode control of unmanned bicycle via ELM and barrier function

Long Chen[1], Zhihui Jin[1], Ke Shao[2], Guangyi Wang[1], Shuping He[3], Vladimir Stojanovic[4], Parisa Arabzadeh Bahri[5] and Hai Wang[5]

[1]School of Electronics and Information, Hangzhou Dianzi University, Hangzhou, China
[2]School of Civil Aviation, Northwestern Polytechnical University, Xi'an, China
[3]School of Electrical Engineering and Automation, Anhui University, Hefei, China
[4]Department of Automatic Control, Robotics and Fluid Technique, University of Kragujevac, Kragujevac, Serbia
[5]School of Engineering and Energy; Centre of Water, Energy & Waste, Murdoch University, Perth, Australia
**Corresponding authors:** Hai Wang; Email: hai.wang@murdoch.edu.au; Ke Shao; Email: kshao@nwpu.edu.cn

**Received:** 18 September 2023; **Revised:** 22 April 2024; **Accepted:** 13 May 2024; **First published online:** 12 September 2024

**Keywords:** integral terminal sliding mode (ITSM); balancing barrier function (BF); unmanned bicycle (UB); extreme learning machine (ELM)

## Abstract

In this paper, an unmanned bicycle (UB) with a reaction wheel is designed, and a second-order mathematical model with uncertainty is established. In order to achieve excellent balancing performance of the UB system, an adaptive controller is designed, which is composed of nominal feedback control, compensating control using extreme learning machine observer and reaching control via integral terminal sliding mode (ITSM) and barrier function (BF)-based adaptive law. Owing to the features of BF-based ITSM (BFITSM), not only any uncertainty or disturbance upper bound is not needed any longer but also the finite-time convergence of the closed-loop system can be ensured with a predefined error bound. Moreover, the BF-based control gain can be adaptively adjusted according to the update of the lumped uncertainty such that the overestimation is removed. The stability analysis of the closed-loop system is given according to Lyapunov theory. Comparable experimental results on an actual UB are carried out to validate the superior balancing performance of the proposed controller.

## 1. Introduction

Unmanned bicycle (UB), which is well known for their ability to maintain balance when steering, has been becoming increasingly popular and have been widely used in rescue and other tasks within a narrow space due to its great flexibility and ability in intelligent transportation [1]. However, to accomplish particular tasks, the major challenging technical issue of UB is to ensure satisfying self-balancing performance in different driving scenarios, especially at low or even zero speeds.

Accurate dynamic modelling is the basis of realizing excellent self-balance of the UB system. Recently, many researches have been carried out from the perspectives of both mathematical models and control approaches [1–5]. For example, in ref. [6], the dynamics of the UB using Lagrange's equations for quasi-coordinates are developed, which considers pure rolling without slipping constraints between the ground and the two wheels. In ref. [7], the dynamics of bicycles such as self-stabilizing models and rear wheel steering models are considered and analysed from the perspective of control. In ref. [8], a dynamic model is presented, which considers the geometric-stabilization mechanisms due to bicycle trail. It is pointed out that the geometry is the most important factor that affects the stability of the bicycle. In ref. [9], the dynamics of the Whipple bicycle is analysed, and a complete non-linear model is constructed, from which the equilibrium point of the bicycle in both straight and circular motions is determined. In ref. [10], the gyrostabilizer is used as the actuator to keep the UB balance, and the

dynamic model of the UB together with the gyrostabilizer is developed using Newton–Euler method. Unfortunately, gyrostabilizers can dramatically increase the bicycle's mass. Inspired by [11], this work installs an independent reaction wheel (RW) in the UB. RW is usually used in spacecraft attitude control due to the advantages of simple structure, low cost and long duration. When the bicycle tilts, a high-performance motor-driven RW actively provides an anti-roll torque, which counteracts the tilting torque and balances the bicycle. Owing to the RW, the model of the UB is changed from a conventional single-input double-output system to a single-input single–output system, and as a result, the balancing control of the UB is greatly simplified.

On the other hand, the superior control strategy is also crucial for the UB self-balance. Many non-linear control strategies have been developed for non-linear systems, such as model-predictive control [12–13], fuzzy control [14–15], robust control [16], adaptive control [17] and sliding mode control (SMC) [18–20]. Among these methods, as a classical non-linear control algorithm, SMC has been widely used in a variety of mechatronic systems due to its fast response, high precision and strong robustness against external disturbances. In ref. [21], a novel adaptive sliding controller based on a robust disturbance observer is designed for non-linear uncertain robotic systems to deal with the tracking control problem. In ref. [22], an adaptive non-singular integral terminal SMC for AUVs is presented to eliminate the need for pre-known uncertainty bounds, which offers the improved tracking accuracy, rapid convergence and robustness against uncertainties and disturbances. In ref. [23], an adaptive fast non-singular integral terminal SMC, based on desired trajectory, is proposed for AUVs, achieving faster convergence rates in AUV dynamics. In ref. [24], an adaptive non-singular terminal sliding mode tracking controller is designed for robotic systems using fuzzy wavelet networks to improve the control performance. In ref. [25], a novel predefined-time barrier function (BF) adaptive SMC strategy for robust control of disturbed systems is designed. This approach ensures that, should an escape event occur at any given time instant, the system trajectory is guaranteed to return to its ultimate bound within a predefined time frame. SMC has also been applied to UB due to its superior performance and strong robustness. In ref. [26], a gyroscopic balancer based on fuzzy SMC is used to control the bicycle, wherein the roll angle is controlled by a backstepping algorithm. In ref. [27], fuzzy SMC is designed, wherein the large uncertainty caused by complex ground conditions is well tackled by the inherent under actuated control scheme. Moreover, in the recent years, many artificial intelligence technologies are applied to the control field. In ref. [28], reinforcement learning is introduced for high-accuracy tracking control of 6-degree-of-freedom (6-DOF) hydraulic robotic manipulators, demonstrating its effectiveness in providing system-level performance guarantees through experimental validation on a 6-DOF platform.

Based on the above discussions, for the purpose of achieving excellent balancing control of the UB, a BF-based adaptive integral terminal sliding mode (BFITSM) control scheme combined with an extreme learning machine (ELM) observer is proposed in this paper. The main contributions of this article are summarized as follows:

1) An adaptive integral terminal sliding mode controller combining ITSM and BF techniques is designed such that the reaching phase can be efficiently eliminated to improve the convergence performance. Since the BF-based adaptive gain is updated according to the lumped uncertainty, overestimation can be effectively suppressed. Moreover, the size of the region that the roll angle tracking error converges to can be exactly predefined. However, the parameter selection of BF is one of the difficulties in the controller design.
2) To counteract the effects of uncertain disturbances and reduce the chattering phenomenon, an ELM observer is developed to estimate the lumped uncertainty. The output weights of the proposed ELM are adaptively adjusted to ensure the Lyapunov stability of the closed-loop control. As such, the estimation of the ELM observer is used as compensating control input to further improve the closed-loop control performance. To achieve better training effect, the value of the $\boldsymbol{O}_i$ should be appropriately chosen. In this work, the output weight $\boldsymbol{O}_i$ is chosen according to the Lyapunov function to keep the control system stable and achieve the excellent estimate.

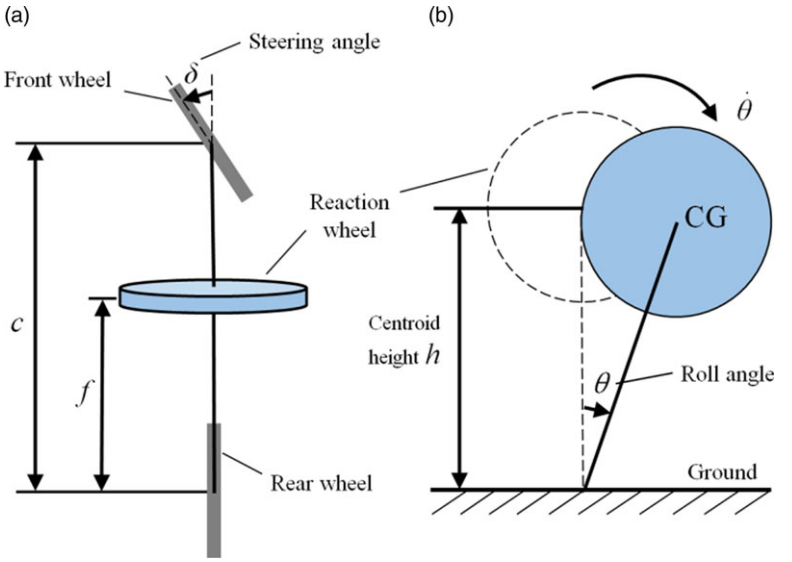


***Figure 1.*** *Bicycle structure. (a) Top view, and (b) Rear view.*

3) Combined with the BF adaptive gain and ELM techniques, a finite-time control strategy that without any disturbance upper bound information and has excellent convergence performance is realized and applied to the UB experimental to verify the effectiveness. Experimental results demonstrate the excellent control performance of the proposed controller.

The reminder of this paper is organized as follows. In Section 2, the uncertain dynamic model of the RW-based UB is presented. An adaptive ITSM controller based on ELM observer is designed in Section 3, and the closed-loop stability analysis is rigorously given in detail. In Section 4, experiment studies on an actual UB are carried out by comparison with conventional control schemes. Section 5 finally concludes the paper.

## 2. Modeling of reaction wheel unmanned bicycle

Fig. 1(a) and 1(b) shows the top and rear views for the RW-based UB system, respectively. The dynamics of the UB can be described by the following second-order differential equation [7]:

$$J\ddot{\theta} = \frac{mfhv}{c}\dot{\delta} + \frac{mhv^2}{c}\delta + mgh\sin(\theta) + d - u \tag{1}$$

For a better illustration, the signification of the notations appeared in Fig. 1 and Eq. (1) are given in Table I.

Since the roll angle of the bicycle is kept within a relatively small range in the process of motion, $\sin(\theta)$ in (1) can be approximated as $\theta$ [29]. For simplification, $\frac{mf}{c}$ and $\frac{mh}{c}$ are denoted as $N$ and $P$, respectively, and $mgh$ is denoted as $M$. Then, at a small roll angle $\theta$, (1) can be rewritten as

$$J\ddot{\theta} = Nv\dot{\delta} + Pv^2\delta + M\theta + d - u \tag{2}$$

Since it is impossible to obtain accurate parameter values in a practical UB system, parametric uncertainties have to be considered in the physical model. The system parameters can be normally divided into a nominal part and an uncertain part as follows [18]:

$$J = J_0 + \Delta J \tag{3}$$

$$N = N_0 + \Delta N \tag{4}$$

***Table I.*** *Notations description.*

| Notations | Signification |
|---|---|
| $J$ | Inertia of the UB |
| $m$ | Total mass of the UB |
| $f$ | Distance from the rear wheel to the mass centrer of the UB |
| $\delta$ | Steering angle of the front wheel relative to the positive direction of UB |
| $c$ | Distance from rear wheel to front wheel |
| $g$ | Gravitational constant |
| $h$ | Height of centre of gravity (CG) from the ground |
| $\theta$ | Roll angle of the UB |
| $v$ | Forward speed of the UB |
| $d$ | Unknown disturbance |
| $u$ | Control input |

$$P = P_0 + \Delta P \tag{5}$$

$$M = M_0 + \Delta M \tag{6}$$

where $J_0$, $N_0$, $P_0$ and $M_0$ are the nominal values determined from preliminary experiments, and $\Delta J$, $\Delta N$, $\Delta P$ and $\Delta M$ are the corresponding model parameter errors, respectively. Then, the dynamical Eq. (2) can be rewritten as

$$J_0\ddot{\theta} = N_0 v\dot{\delta} + P_0 v^2\delta + M_0\theta + l - u \tag{7}$$

where $l$ is the lumped uncertainty, which is given by

$$l = d + \Delta N v\dot{\delta} + \Delta P v^2\delta + \Delta M\theta - \Delta J\ddot{\theta} \tag{8}$$

According to Appendix A, the closed-loop control signal is chosen to be upper bounded by the following polynomial function in this paper:

$$|u| < \zeta_0 + \zeta_1|\theta| + \zeta_2|\dot{\theta}| \tag{9}$$

Then the lumped uncertainty is bounded by [30], the detailed derivation process is given in Appendix B:

$$|l| < \bar{l} \tag{10}$$

where $\bar{l}$ is the upper bound of $l$, given by

$$\bar{l} = \mu_0 + \mu_1|\theta| + \mu_2|\dot{\theta}| \tag{11}$$

where $\zeta_0$, $\zeta_1$, $\zeta_2$, $\mu_0$, $\mu_1$ and $\mu_2$ are unknown positive constants.

The control objective is to keep the roll angle of the UB within a small range under the impact of system uncertainty. To balance the UB, an appropriate reaction force $u$ can be produced such that the roll angle $\theta$ can be retained to be zero with high precision, fast response and strong robustness.

**Remark 1.** In practice, it is quite difficult to obtain the accurate bound information of the lumped uncertainty in (11). To deal with the effect of the lumped uncertainty, a conservatively large constant is usually selected in conventional SMC systems. However, the overly large bound may lead to severe control chattering and large control efforts. Although boundary layer technique can be normally used to alleviate this phenomenon, the control precision will be accordingly degraded. In this paper, in order to achieve better control performance, an ELM observer and BF-based adaptive ITSM controller will be designed such that not only the need for the prior uncertainty information can be eliminated wherein the control gain will be adaptively adjusted but also the control precision can be exactly ensured by tuning parameters.

## 3. Design of controller

In this section, we develop an ELM-based BFITSM (ELM-BFITSM) controller for the RW-based UB system. First, a feedback control component using ITSM is designed without considering the system uncertainty. Then, the compensating control component based on ELM and the reaching control component using BF-based adaptive law are designed to deal with the lumped uncertainty.

### *3.1. Design of ELM-BFITSM*

In this work, the tracking error $e$ is defined as

$$e = \theta - \theta_d \tag{12}$$

where $\theta_d = 0$ is the target roll angle which equals to zero under absolutely balanced state. Then, according to Eq. (7), the second derivative of error $e$ can be obtained as follows when $\theta_d = 0$:

$$\ddot{e} = \ddot{\theta} = \frac{1}{J_0}\left(N_0 v\dot{\delta} + P_0 v^2 \delta + M_0 \theta + l - u\right) \tag{13}$$

To derive the controller, a novel integral terminal sliding mode variable $s$ is designed as [31–32]:

$$s = \dot{e} + \alpha_1 e + \alpha_2 e_I \tag{14}$$

$$e_I = \begin{cases} e_I(0), & t = 0 \\ \int_0^t e^{\frac{q_1}{q_2}} d\tau & t > 0 \end{cases} \tag{15}$$

where $\alpha_1 > 0$ and $\alpha_2 > 0$ are constants, $q_1$ and $q_2$ are odd integers satisfying $q_2 > q_1 > 0$ to keep $e^{q_1/q_2}$ a real number and ensure finite time convergence of $e$ [33]. The initial value $e_I(0)$ is set as

$$e_I(0) = \frac{\dot{e}(0) + \alpha_1 e(0)}{\alpha_2} \tag{16}$$

where $e(0)$ and $\dot{e}(0)$ are the initial values of the actual error status available for eliminating the reaching time. Ignoring the lumped uncertainty and combining $\dot{s} = 0$ with (13), the equivalent control input of the proposed sliding mode controller can be designed as

$$u_0 = N_0 v\dot{\delta} + P_0 v^2 \delta + M_0 \theta + J_0(\alpha_1 \dot{e} + \alpha_2 \dot{e}_I) \tag{17}$$

Next, based on the ELM technique, the compensating control input $u_1$ of the closed-loop control system is designed as

$$u_1 = \hat{l} \tag{18}$$

where $\hat{l}$ is the estimate value of the lumped uncertainty via ELM that will be given later.

Furthermore, in order to achieve that the system converges from arbitrary initial state to the preset sliding mode surface quickly, a reaching control input is introduced as follows:

$$u_2 = J_0 \hat{k}\,\mathrm{sign}(s) \tag{19}$$

where $\hat{k}$ represents an adaptive control gain.

The schematic diagram of the proposed ELM-BFITSM is shown in Fig. 2. In this paper, we define a small positive number $\varepsilon$ by which to define the region of $(-\varepsilon, \varepsilon)$ that the sliding variable will converge to [34–35]. If the initial value of the sliding mode variable $s$ is outside the region $[-\frac{\varepsilon}{2}, \frac{\varepsilon}{2}]$, namely $|s(0)| > \frac{\varepsilon}{2}$, it will converge to the region under a monotonically increasing gain. It defines $\bar{t}$ as the time instant when

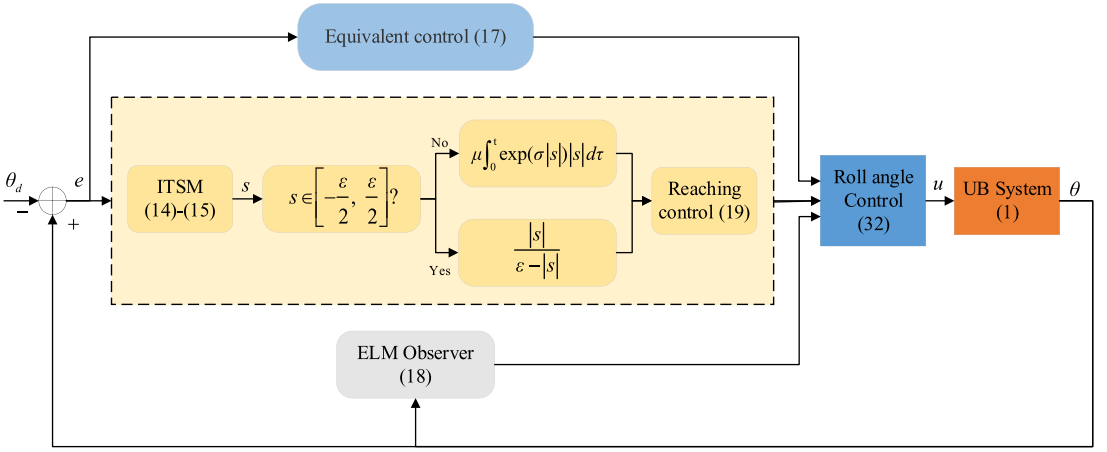


***Figure 2.*** *Schematic diagram of the proposed ELM-BFITSM controller for UB.*

the initial state firstly converges into the above region. After the initial value of $s$ is in this region, namely $|s(0)| \leq \frac{\varepsilon}{2}$, a BF-based gain will be activated. Explicitly, the proposed adaptive law is designed as

$$\hat{k} = \begin{cases} \mu \int_0^t \exp(\sigma |s|)\, |s|\, d\tau, & \text{for } 0 \leq t \leq \bar{t} \\ f_b(s), & \text{for } t > \bar{t} \end{cases} \tag{20}$$

where the parameters $\sigma \geq 0$, $\mu > 0$, and the initial value of $\hat{k}(0) > 0$. $\bar{t}$ is the time instant that the sliding variable converges to the region of $[-\frac{\varepsilon}{2}, \frac{\varepsilon}{2}]$, i.e., $\left|s(\bar{t})\right| = \frac{\varepsilon}{2}$. $f_b(s)$ is the BF which is defined as

$$f_b(s) = \frac{|s|}{\varepsilon - |s|} \tag{21}$$

**Remark 2.** When $t \leq \bar{t}$, under $\hat{k} = \mu \int_0^t \exp(\sigma |s|)|s|d\tau$, the sliding variable $s$ will quickly converge to the region $[-\frac{\varepsilon}{2}, \frac{\varepsilon}{2}]$. When $t > \bar{t}$, $\hat{k}$ is updated by the BF function $f_b(s)$, whose output changes with the variation of $s$. The reason why BF can reduce the chattering effect compared to constant gain is that: if $|s|$ gradually increases in $[0, \varepsilon)$, $f_b(s)$ will also accordingly increase to a large number to pull $|s|$ back to the predefined region; if $|s|$ reaches the sliding surface, $\hat{k}$ will reduce to a small number. Meanwhile, in this way, it can guarantee that the control gain of the ELM-BFITSM is not overestimated.

**Remark 3.** In conventional SMC, an overlarge constant $k$ is usually selected as the gain of reaching law to keep the system stable, which requires the upper bound of $l$ at advance and leads to a serious chattering problem. The reason is that when $s$ crosses 0 frequently, the control law changes discontinuously in two values of $\pm k$. In this paper, because of the introduction of BF, the final $u_2$ becomes continuous. Since the sliding variable $s$ is changing continuously, the $f_b(s)$ will be continuous either. It can be seen from Fig. 3 that when $s$ crosses 0, the final $u_2$ is continuously changed despite the involved signum function. Therefore, the signal chattering in control input can be effectively reduced. Moreover, $l$ is compensated by ELM ($u_1$) such that the control gain needs to be greater than the estimation error and does not need to be greater than the upper bound, which will effectively reduce the chattering problem. Moreover, the BF function will further reduce chattering as we discussed above.

### *3.2. Design of ELM observer*

The architecture of the ELM observer is shown in Fig. 4. The weight and bias of the input layer of ELM proposed by Huang [36] are randomly generated without reverse adjustment, and the output layer

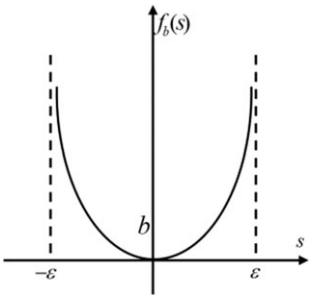


***Figure 3.*** *The scheme of barrier function.*

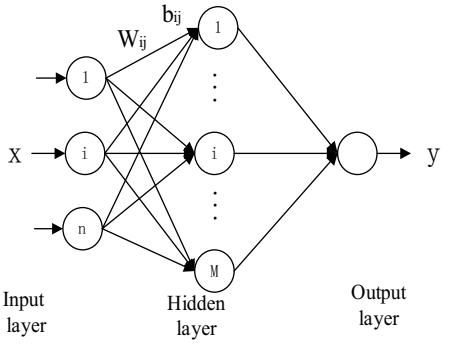


***Figure 4.*** *ELM observer architecture.*

weights are calculated directly through a least squares solution. Conversely, the radial basis function (RBF) necessitates the employment of iterative methodologies to ascertain the optimal values for the centres, widths, and weights of the network and require an iterative optimization process to adjust their parameters, which can be more time consuming. Therefore, compared with the conventional neural network algorithm, ELM has a lower algorithm complexity and a faster learning speed. The training process of ELM is mainly divided into two steps.

**Step 1: Random generation of input weights $W_i$ and bias $b_i$**

The output of the hidden layer is the input multiplied by the corresponding weight plus its deviation, and then it is summed by a non-linear function (activation function) of all the nodes. When the sample $X_1$ is input, the corresponding hidden layer output is as follows:

$$\boldsymbol{h}_i(X_1) = \boldsymbol{G}(W_i X_1 + b_i)\ i = 1, 2, \cdots, L \tag{22}$$

where $\boldsymbol{h}_i(X_1)$ is the output of the $i$-th hidden layer node when the input sample $X_1$ is input, and $\boldsymbol{G}(\cdot)$ is the activation function. We can obtain the output matrix $\boldsymbol{H}(X)$ of the hidden layer:

$$\begin{aligned} \boldsymbol{H} &= \begin{pmatrix} \boldsymbol{h_1}(X_1) & \cdots & \boldsymbol{h_L}(X_1) \\ \cdots & \ddots & \cdots \\ \boldsymbol{h_1}(X_U) & \cdots & \boldsymbol{h_L}(X_U) \end{pmatrix} \\ &= \begin{pmatrix} \boldsymbol{G}(X_1 W_1 + b_1) & \cdots & \boldsymbol{G}(X_1 W_L + b_L) \\ \vdots & \ddots & \vdots \\ \boldsymbol{G}(X_U W_1 + b_1) & \cdots & \boldsymbol{G}(X_U W_L + b_L) \end{pmatrix} \in R^{U \times L} \end{aligned} \tag{23}$$

The network output of the feedforward neural network ELM with a single hidden layer is as follows:

$$\boldsymbol{HO} = \boldsymbol{T} \tag{24}$$

where $\boldsymbol{T} = \left[\boldsymbol{t}_1^{\mathrm{T}}, \boldsymbol{t}_2^{\mathrm{T}}, \cdots, \boldsymbol{t}_U^{\mathrm{T}}\right]^{\mathrm{T}} \in R^{U\times m}$, and $\boldsymbol{O}$ is the output weight, which will be obtained in Step 2.

**Step 2: Obtain the output weight $\boldsymbol{O}_i$ by minimizing the loss function**

The goal of single hidden layer neural network learning is to minimize the output error, which is the difference between the network output $\boldsymbol{T}$ and the objective function $\boldsymbol{Y}$. In order to achieve better training effect, it needs to choose the value of the $\boldsymbol{O}_i$. That is, the weight $\boldsymbol{O}_i$ that connects the hidden layer. The output layer is solved by minimizing the approximate square variance. The objective function is as follows:

$$\|\boldsymbol{T}^* - \boldsymbol{Y}\| = \mathbf{min}\ \ \|\boldsymbol{T} - \boldsymbol{Y}\| \tag{25}$$

The above equation can also be written in the following form:

$$\|\boldsymbol{H}(\boldsymbol{X}, \boldsymbol{W}, \boldsymbol{b})\, \boldsymbol{O}^* - \boldsymbol{Y}\| = \min_{\boldsymbol{O}} \|\boldsymbol{H}(\boldsymbol{X}, \boldsymbol{W}, \boldsymbol{b})\, \boldsymbol{O} - \boldsymbol{Y}\| \tag{26}$$

where $\boldsymbol{O}^*$ is the optimal solution that requires, and it can be solved by the following equation:

$$\boldsymbol{O}^* = \boldsymbol{H}^{\dagger}\boldsymbol{Y} \tag{27}$$

where $\boldsymbol{H}^{\dagger}$ is the generalized inverse of $\boldsymbol{H}$.

Therefore, the estimated lumped uncertainty $\hat{l}$ in (18) can be obtained via the ELM mechanism modelled as

$$\hat{l} = \boldsymbol{H}(\boldsymbol{x}, \boldsymbol{w}, \boldsymbol{b})\, \hat{\boldsymbol{O}} \tag{28}$$

where $X_{in}(0) = [\theta, \dot{\theta}]^{\mathrm{T}}$ is input vector and $\hat{\boldsymbol{O}}$ is an design function. The output matrix of the ELM is also designed as a piecewise function as shown below:

$$\dot{\hat{\boldsymbol{O}}}^T = \begin{cases} \rho s \boldsymbol{H}, & \text{for } 0 \le t \le \bar{t} \\ J_0 \rho \left( \dfrac{s}{J_0} + \dfrac{\hat{k}}{J_0} \dfrac{\varepsilon}{(\varepsilon - |s|)^2} \mathrm{sign}(s) \right) \boldsymbol{H}, & \text{for } t > \bar{t} \end{cases} \tag{29}$$

where $\rho$ is a positive constant and $\hat{k}$ is the adaptive gain given in (20). It should be noted that the initial condition of $\dot{\hat{\boldsymbol{O}}}^T$ depends on the initial condition $X_{in}(0) = [\theta(0), \hat{\theta}(0)]^{\mathrm{T}}$. In real applications, to keep a balanced state, we often select the initial condition as $\theta(0) = \dot{\theta}(0) = 0$.

The estimate value of lumped uncertainty is approximated by

$$l = \boldsymbol{H}\boldsymbol{O}^* + \zeta \tag{30}$$

where $l$ is the ideal output of single hidden-layer feedforward network, $\boldsymbol{O}^*$ is the optimal constant output weight vector, and $\zeta$ is the approximation error which is assumed to be bounded by

$$\max\left\{ |J_0{}^{-1}\tilde{l}|, |J_0{}^{-1}\zeta| \right\} < k \tag{31}$$

where $\tilde{l} = l - \hat{l}$, and $k$ denotes the bound of the disturbance that is not compensated.

**Remark 4.** In this article, the inputs of ELM are chosen as $X_{in} = [\theta, \dot{\theta}]^{\mathrm{T}}$. The concealed layer input weights and biases are generated randomly according to the Gaussian distribution, and the output weights is obtained from the generalized inverse matrix. Different from the conventional ELM algorithm proposed for classification problems [37–38], the proposed ELM algorithm estimates the lumped uncertainty and takes the estimate value as the compensating control input as shown in (18).

### *3.3. Stability analysis*

**Theorem 1:** *For system (2), if the sliding function is chosen as (14) and the controller is designed as*

$$u = u_0 + u_1 + u_2 \tag{32}$$

*where $u_0$ is the equivalent control input (17), $u_1$ is the compensating control input (18) obtained by the ELM observer (28), and $u_2$ is the reaching control input (19). The proposed controller effectively avoids the singularity problem. Then, under the proposed controller (32), the sliding variable converges to $(-\varepsilon, \varepsilon)$ and the tracking error converges to $\left(-\frac{\varepsilon}{\alpha_1}, \frac{\varepsilon}{\alpha_1}\right)$, both in finite time.*

***Proof***: According to (20), the proof will be accomplished by two steps, i.e., $0 \le t \le \bar{t}$ and $t > \bar{t}$. □

**Step 1. $0 \le t \le \bar{t}$ for the control law (20)**

Select a Lyapunov function $V_1$ as

$$V_1 = L_1 + \frac{\tilde{\boldsymbol{O}}^T \tilde{\boldsymbol{O}}}{2J_0\rho} \tag{33}$$

where $L_1 = \frac{s^2}{2} + \frac{\tau}{2}\tilde{k}^2$ with $\tau > 1$, $\tilde{\boldsymbol{O}}$ is the estimation output error of the ELM output layer given by:

$$\tilde{\boldsymbol{O}} = \boldsymbol{O}^* - \hat{\boldsymbol{O}} \tag{34}$$

and $\tilde{k}$ is the adaptive error $\tilde{k} = \hat{k} - k$.

Taking the derivative of $V_1$ with respect to time, we obtain:

$$\begin{aligned}
\dot{V}_1 &= s\dot{s} + \tau\tilde{k}\dot{\tilde{k}} + \frac{1}{J_0\rho}\dot{\tilde{\boldsymbol{O}}}^T\tilde{\boldsymbol{O}} \\
&= s(\ddot{e} + \alpha_1\dot{e} + \alpha_2\dot{e}_I) + \tau\tilde{k}\dot{\tilde{k}} + \frac{1}{J_0\rho}\dot{\tilde{\boldsymbol{O}}}^T\tilde{\boldsymbol{O}} \\
&= s\left(\frac{1}{J_0}\left(N_0 v\dot{\delta} + P_0 v^2\delta + M_0\theta + l - u_0 - u_1 - u_2\right) + \alpha_1\dot{e} + \alpha_2\dot{e}_I\right) + \tau\tilde{k}\dot{\tilde{k}} + \frac{1}{J_0\rho}\dot{\tilde{\boldsymbol{O}}}^T\tilde{\boldsymbol{O}}
\end{aligned}$$

Next, substituting (17), (18) and (19) into the above equation and combining (28) with (30) yield:

$$\begin{aligned}
\dot{V}_1 &= \frac{s}{J_0}\left(l - \hat{l} - J_0\hat{k}\,\mathrm{sign}(s)\right) + \tau\tilde{k}\dot{\tilde{k}} + \frac{1}{J_0\rho}\dot{\tilde{\boldsymbol{O}}}^T\tilde{\boldsymbol{O}} \\
&= \frac{s}{J_0}\left(\boldsymbol{H}(\boldsymbol{O}^* - \hat{\boldsymbol{O}}) + \zeta - J_0\hat{k}\,\mathrm{sign}(s)\right) + \tau\tilde{k}\dot{\tilde{k}} + \frac{1}{J_0\rho}\dot{\tilde{\boldsymbol{O}}}^T\tilde{\boldsymbol{O}} \\
&= \frac{s}{J_0}\boldsymbol{H}\tilde{\boldsymbol{O}} + \frac{1}{J_0\rho}\dot{\tilde{\boldsymbol{O}}}^T\tilde{\boldsymbol{O}} + \frac{s}{J_0}(\zeta - J_0\hat{k}\,\mathrm{sign}(s)) + \tau\tilde{k}\dot{\tilde{k}} \\
&= \left(\frac{s}{J_0}\boldsymbol{H} + \frac{1}{J_0\rho}\dot{\tilde{\boldsymbol{O}}}^T\right)\tilde{\boldsymbol{O}} + \frac{s}{J_0}\left(\zeta - J_0\hat{k}\,\mathrm{sign}(s)\right) + \tau\tilde{k}\dot{\tilde{k}}
\end{aligned} \tag{35}$$

If $\dot{\hat{\boldsymbol{O}}}^T$ in (28) is chosen as

$$\dot{\hat{\boldsymbol{O}}}^T = \rho s\boldsymbol{H} \tag{36}$$

The disturbance in UB system is slow time varying, so there exists a slow-changing optimal parameter $\boldsymbol{O}^*$, whose derivative is a very small number such that $\dot{\tilde{\boldsymbol{O}}}^T = -\dot{\hat{\boldsymbol{O}}}^T = -\rho s\boldsymbol{H}$. Then, considering (20), (35) can be rewritten as

$$\begin{aligned}\dot{V}_1 &= \frac{1}{J_0}\left(\zeta s - J_0 s\hat{k}\text{sign}(s)\right) + \tau\tilde{k}\dot{\hat{k}} \\ &= \frac{1}{J_0}\left(\zeta s - J_0\hat{k}|s|\right) + \tau(\hat{k}-k)\mu\exp(\sigma|s|)\,|s| + (k-k)\,|s| \\ &\le \frac{1}{J_0}\left(|\zeta|\,|s| - J_0\hat{k}|s|\right) + \tau(\hat{k}-k)\mu\exp(\sigma|s|)\,|s| + (k-k)\,|s| \\ &\le \frac{1}{J_0}\left(|\zeta|\,|s| - J_0 k|s|\right) + \tau(\hat{k}-k)\mu\exp(\sigma|s|)\,|s| - (\hat{k}-k)\,|s| \\ &= -\frac{1}{J_0}\left(J_0 k|s| - |\zeta|\,|s|\right) + (\hat{k}-k)\,|s|\,(\tau\mu\exp(\sigma|s|) - 1)\end{aligned}$$

Till to now, it has been proved that for $0 \le t \le \bar{t}$ the adaptive gain $\hat{k} = \eta\int_0^t \exp(\alpha|s|)|s|d\tau$ is bounded [39]. Then, defining $k$ as the upper bound of $\hat{k}$ that satisfies (31), we get $\hat{k} - k = -|k-\hat{k}|$, and as a result,

$$\begin{aligned}\dot{V}_1 &\le -\frac{1}{J_0}\left(J_0 k|s| - |\zeta|\,|s|\right) - \left|k-\hat{k}\right|\,|s|\,(\tau\mu\exp(\sigma|s|) - 1) \\ &= -\left(k - \left|J_0^{-1}\zeta\right|\right)|s| - (\tau\mu\exp(\sigma|s|) - 1)\,|s|\left|\tilde{k}\right| \end{aligned} \tag{37}$$

Recalling (31) and considering that for any $\mu$ and $\sigma$ there exists a positive number $\tau$ such that $\tau\mu\exp(\sigma|s|) > 1$, we have

$$\dot{V}_1 < 0$$

for any $|s(t)| > \frac{\varepsilon}{2}$, i.e., $\tilde{\boldsymbol{O}} \to 0$ which implies the convergence of the estimation. Particularly, for the Lyapunov function $L_1$, by following a similar procedure, we can obtain:

$$\dot{L}_1 \le -\left(k - \left|J_0^{-1}\tilde{l}\right|\right)|s| - (\tau\mu\exp(\sigma|s|) - 1)\,|s|\left|\tilde{k}\right|$$

By defining the following symbols:

$$\begin{aligned}\varrho_1 &= k - \left|J_0^{-1}\tilde{l}\right| \\ \varrho_2 &= (\tau\mu\exp(\sigma|s|) - 1)\,|s|\end{aligned}$$

where $\varrho_1, \varrho_2 > 0$, we further obtain:

$$\begin{aligned}\dot{L}_1 &\le -\varrho_1|s| - \varrho_2\left|\tilde{k}\right| \\ &= -\varrho_1\sqrt{2}\frac{|s|}{\sqrt{2}} - \varrho_2\sqrt{2}\frac{\left|\tilde{k}\right|}{\sqrt{2}} \\ &\le -\vartheta_1\left(\frac{|s|}{\sqrt{2}} + \frac{\left|\tilde{k}\right|}{\sqrt{2}}\right) \\ &\le -\vartheta_1 L_1^{\frac{1}{2}}\end{aligned} \tag{38}$$

where $\vartheta_1 = \min\{\sqrt{2}\varrho_1, \sqrt{2}\varrho_2\}$. Since $\vartheta_1 > 0$, there must exist a positive constant $T_1$ such that:

$$T_1 \le \vartheta_1, \forall\,|s(t)| > \frac{\varepsilon}{2} \tag{39}$$

From (38), we have

$$\dot{L}_1 \le -T_1 L_1^{\frac{1}{2}} \tag{40}$$

Therefore, the inequality (40) satisfies the finite time stability criterion in Appendix C, which shows that there exists a finite time $\bar{t}$ for the sliding variable to converge to $[-\frac{\varepsilon}{2}, \frac{\varepsilon}{2}]$ which is bounded by

$$\bar{t} \leq \frac{L_1^{\frac{1}{2}}(0) - L_1^{\frac{1}{2}}(\bar{t})}{0.5T_1} \tag{41}$$

**Step 2: $t > \bar{t}$ for the control law (20).**

To prove the stability, the following intermediate variable is introduced:

$$\varnothing = \varepsilon \frac{|\zeta|}{|\zeta| + J_0} < \varepsilon \tag{42}$$

In order to prove that the sliding variable $s$ will be retained in the region of $(-\varepsilon, \varepsilon)$ thereafter, we will first prove that $|s(t)| \leq \varnothing < \varepsilon$ will be ensured in finite time $t_s$ from $\left|s(\bar{t})\right| = \frac{\varepsilon}{2} > \varnothing$. Considering the case of $\left|s(\bar{t})\right| = \frac{\varepsilon}{2} > \varnothing$, a Lyapunov function $V_2$ is defined as

$$V_2 = L_2 + \frac{\tilde{\boldsymbol{O}}^T \tilde{\boldsymbol{O}}}{2J_0\rho} \tag{43}$$

where $L_2 = \frac{s^2}{2} + \frac{1}{2}\hat{k}^2$. Taking the derivative of $V_2$ with respect to time yields.

$$\dot{V}_2 = s\dot{s} + \hat{k}\dot{\hat{k}} + \frac{1}{J_0\rho}\dot{\tilde{\boldsymbol{O}}}^T\tilde{\boldsymbol{O}}$$

According to Eqs. (17)-(20) and following a similar procedure in Step 1), we obtain:

$$\begin{aligned}
\dot{V}_2 &= \frac{s}{J_0}\left(l - J_0\hat{k}\text{sign}(s) - \hat{l}\right) + \hat{k}\dot{\hat{k}} + \frac{1}{J_0\rho}\dot{\tilde{\boldsymbol{O}}}^T\tilde{\boldsymbol{O}} \\
&= \frac{s}{J_0}\left(l - J_0\hat{k}\text{sign}(s) - \hat{l}\right) + \hat{k}\frac{\varepsilon}{(\varepsilon - |s|)^2}\text{sign}(s)\dot{s} + \frac{1}{J_0\rho}\dot{\tilde{\boldsymbol{O}}}^T\tilde{\boldsymbol{O}} \\
&= \left(\frac{s}{J_0} + \frac{\hat{k}}{J_0}\frac{\varepsilon}{(\varepsilon - |s|)^2}\text{sign}(s)\right)\left(l - J_0\hat{k}\text{sign}(s) - \hat{l}\right) + \frac{1}{J_0\rho}\dot{\tilde{\boldsymbol{O}}}^T\tilde{\boldsymbol{O}}
\end{aligned}$$

where the fact of $\dot{s} = \frac{1}{J_0}\left(l - J_0\hat{k}\text{sign}(s) - \hat{l}\right)$ as indicated by (35) has been used. Furthermore, combining (28) with (30), we have

$$\begin{aligned}
\dot{V}_2 &= \left(\frac{s}{J_0} + \frac{\hat{k}}{J_0}\frac{\varepsilon}{(\varepsilon - |s|)^2}\text{sign}(s)\right)\left(\boldsymbol{H}\tilde{\boldsymbol{O}} + \zeta - J_0\hat{k}\text{sign}(s)\right) + \frac{1}{J_0\mu}\dot{\tilde{\boldsymbol{O}}}^T\tilde{\boldsymbol{O}} \\
&= \left(\left(\frac{s}{J_0} + \frac{\hat{k}}{J_0}\frac{\varepsilon}{(\varepsilon - |s|)^2}\text{sign}(s)\right)\boldsymbol{H} + \frac{1}{J_0\rho}\dot{\tilde{\boldsymbol{O}}}^T\right)\tilde{\boldsymbol{O}} + \left(\frac{s}{J_0} + \frac{\hat{k}}{J_0}\frac{\varepsilon}{(\varepsilon - |s|)^2}\text{sign}(s)\right)\left(\zeta - J_0\hat{k}\text{sign}(s)\right)
\end{aligned} \tag{44}$$

If $\dot{\hat{\boldsymbol{O}}}^T$ in (28) is chosen as

$$\dot{\hat{\boldsymbol{O}}}^T = J_0\rho\left(\frac{s}{J_0} + \frac{\hat{k}}{J_0}\frac{\varepsilon}{(\varepsilon - |s|)^2}\text{sign}(s)\right)\boldsymbol{H} \tag{45}$$

such that:

$$\dot{\tilde{\boldsymbol{O}}}^T = -\dot{\hat{\boldsymbol{O}}}^T = -J_0\rho\left(\frac{s}{J_0} + \frac{\hat{k}}{J_0}\frac{\varepsilon}{(\varepsilon - |s|)^2}\text{sign}(s)\right)\boldsymbol{H}$$

Then, (43) can be expressed as

$$\begin{aligned}\dot{V}_2 &= \left(\frac{s}{J_0} + \frac{\hat{k}}{J_0}\frac{\varepsilon}{(\varepsilon - |s|)^2}\text{sign}(s)\right)\left(\zeta - J_0\hat{k}\text{sign}(s)\right)\\ &= \frac{1}{J_0}\left(\zeta s - J_0\hat{k}|s|\right) + \frac{\hat{k}}{J_0}\frac{\varepsilon}{(\varepsilon - |s|)^2}\left(\zeta\,\text{sign}(s) - J_0\hat{k}\right)\\ &\le -\frac{1}{J_0}\left(J_0\hat{k}|s| - |\zeta|\,|s|\right) - \frac{\hat{k}}{J_0}\frac{\varepsilon}{(\varepsilon - |s|)^2}\left(J_0\hat{k} - |\zeta|\right)\\ &= -\left(\hat{k} - \left|J_0^{-1}\zeta\right|\right)|s| - \frac{\varepsilon}{(\varepsilon - |s|)^2}\left(\hat{k} - \left|J_0^{-1}\zeta\right|\right)\hat{k}\end{aligned} \tag{46}$$

According to (42), one can obtain that $\hat{k}(s) > \hat{k}(\varnothing) = |J_0^{-1}\zeta|$. Then, we obtain:

$$\dot{V}_2 < 0$$

for any $\varnothing < |s(t)| \le \frac{\varepsilon}{2}$ which demonstrates that the estimation is converging. Moreover, by defining another intermediate variable $\varnothing' = \varepsilon\frac{|\tilde{l}|}{|\tilde{l}|+J_0}$ and following a similar procedure, it can be obtained that:

$$\dot{L}_2 \le -\left(\hat{k} - \left|J_0^{-1}\tilde{l}\right|\right)|s| - \frac{\varepsilon}{(\varepsilon - |s|)^2}\left(\hat{k} - \left|J_0^{-1}\tilde{l}\right|\right)\hat{k}$$

Define the following symbols:

$$\varrho_1 = \hat{k} - \left|J_0^{-1}\tilde{l}\right| \tag{47}$$

$$\varrho_2 = \frac{\varepsilon}{(\varepsilon - |s|)^2}\left(\hat{k} - \left|J_0^{-1}\tilde{l}\right|\right) \tag{48}$$

which are both positive since $\hat{k}(s) > \hat{k}(\varnothing') = |J_0^{-1}\tilde{l}|$. Then, we have

$$\begin{aligned}\dot{L}_2 &\le -\varrho_1|s| - \varrho_2\hat{k}\\ &= -\varrho_1\sqrt{2}\frac{|s|}{\sqrt{2}} - \varrho_2\sqrt{2}\frac{1}{\sqrt{2}}\hat{k}\\ &\le -\vartheta_2\left(\frac{|s|}{\sqrt{2}} + \frac{1}{\sqrt{2}}\hat{k}\right)\\ &\le -\vartheta_2 L_2^{\frac{1}{2}}\end{aligned} \tag{49}$$

where $\vartheta_2 = \min\{\sqrt{2}\varrho_1, \sqrt{2}\varrho_2\}$. Since $\vartheta_2 > 0$, there must exist a positive constant $T_2$ such that:

$$T_2 \le \vartheta_2, \forall\varnothing < |s(t)| \le \frac{\varepsilon}{2} \tag{50}$$

From (49), we have

$$\dot{L}_2 \le -T_2 L_2^{\frac{1}{2}} \tag{51}$$

Therefore, the inequality (51) satisfies the finite time stability criterion in Appendix C, which shows that there exists a finite time $\bar{t}$ for the sliding variable to converge to [-∅, ∅] which is bounded by

$$t_s \le \frac{L_2^{\frac{1}{2}}(\bar{t}) - L_2^{\frac{1}{2}}(\bar{t} + t_s)}{0.5T_2} \tag{52}$$

According to [34–35], the sliding variable converges to $|s(t)| \le \varnothing < \varepsilon$ in the finite time of $t = \bar{t} + t_s$ and will remain in that region $(-\varepsilon, \varepsilon)$. Furthermore, according to Appendix D, because of the ITSM (14)-(15), the tracking error $e$ will also be bounded in $|e| < \frac{\varepsilon}{\alpha_1}$.

***Table II.*** *Parameters of controllers.*

| Control method | Parameters of sliding mode | Parameters of reaching law |
|---|---|---|
| ITSM | $\alpha_1 = 2.4, \alpha_2 = 1,$ $q_1 = 3, q_2 = 5.$ | $k_1 = 500$ |
| AITSM | $\alpha_1 = 2.4, \alpha_2 = 1,$ $q_1 = 3, q_2 = 5.$ | $k_2 = 300, \sigma = 0.3,$ |
| BFITSM | $\alpha_1 = 2.4, \alpha_2 = 1,$ $q_1 = 3, q_2 = 5.$ | $\varepsilon = 0.05, \mu = 1000,$ $\sigma = 2.5$ |
| ELM-BFITSM | $\alpha_1 = 2.4, \alpha_2 = 1,$ $q_1 = 3, q_2 = 5, L = 5, \rho = 0.1.$ | $\varepsilon = 0.05, \mu = 1000,$ $\sigma = 2.5$ |

Here completes the proof.

**Remark 5.** The convergence of the sliding variable $s$ is divided into two steps: $\bar{t}$ represents the convergence time from the initial state to $\left|s(\bar{t})\right| = \frac{\varepsilon}{2} > \varnothing$ and $t_s$ represents the consumed time to further converge to $|s(t)| \leq \varnothing < \varepsilon$. After the sliding variable converges, namely $|s| \leq \varnothing$, the gain is finally bounded by $\hat{k}(s) \leq f_b(\varnothing) = |J_0{}^{-1}\zeta|$ as implied by (21). It can be seen from (42) that $\varnothing$ accordingly increases (decreases) as the disturbance increases (decreases), and as a result, the tracking error can be limited as small as possible.

**Remark 6.** From (31), it can be concluded that when $s$ changes from 0 to $s = s_2 > 0$, $\hat{\boldsymbol{O}}$ in (30) needs to increase, so that $\zeta$ approaches 0. At the same time, $\hat{k}$ in (46) will also increase because of (20), therefore $\hat{\boldsymbol{O}}$ will increase. As a result, the disturbance compensation for the ELM observer can be more accurate.

### *3.4. Control parameter selection*

The unmodelled dynamics, external disturbance and measurement noise in a practical system require that appropriate control parameters should be synthetically selected to balance the control speed, precision and signal smoothness. The parameters of ELM-BFITSM are shown in Table II.

1) Selections of $\alpha_1, \alpha_2, q_1, q_2 : \alpha_1$ affect the convergence rate of tracking error: the larger the value of $\alpha_1$ is, the faster the error will converge. However, an excessive $\alpha_1$ will increase the control amplitude as shown in (17). The integral term of the sliding variable is used to suppress the steady-state error, and the integral coefficient $\alpha_2$ is usually a small constant. $q_1/q_2$ will also affect the convergence rate of the error. Usually, $q_1$ and $q_2$ are odd integers, and $q_1/q_2$ is less than 1. In our experiment, we chose $\alpha_1 = 2.4$, $\alpha_2 = 1$, $q_1 = 3$, and $q_2 = 5$.
2) Selections of $\varepsilon$, $\sigma$, $\mu$: The parameter $\varepsilon$ defines the convergence region of the tracking error. A smaller $\varepsilon$ implies a better control precision but too small $\varepsilon$ may cause control input saturation and lead to chattering problem. In the adaptive law (20), appropriate $\mu$ and $\sigma$ should be selected in order to make $s$ reach the region faster with an acceptable chattering. $\varepsilon = 0.05$, $\mu = 1000$, and $\sigma = 2.5$ are selected.
3) Selections of $L$, $\rho$: The number of neural nodes $L$ in the hidden layer affects the estimation accuracy: the more the number of neural nodes in the hidden layer is, the more accurate the tracking result will be. However, considering that the calculation capacity of the STM32 microcontroller adopted in our bicycle is limited, the number of $L$ cannot be selected to be too large. The learning rate $\rho$ affects the estimation rate of uncertainty as shown in (36) and (45). A larger $\rho$ value can get a faster estimation result. However, too large $\rho$ value may also cause severe chattering. Finally, we chose $L = 5$ and $\rho = 0.1$.

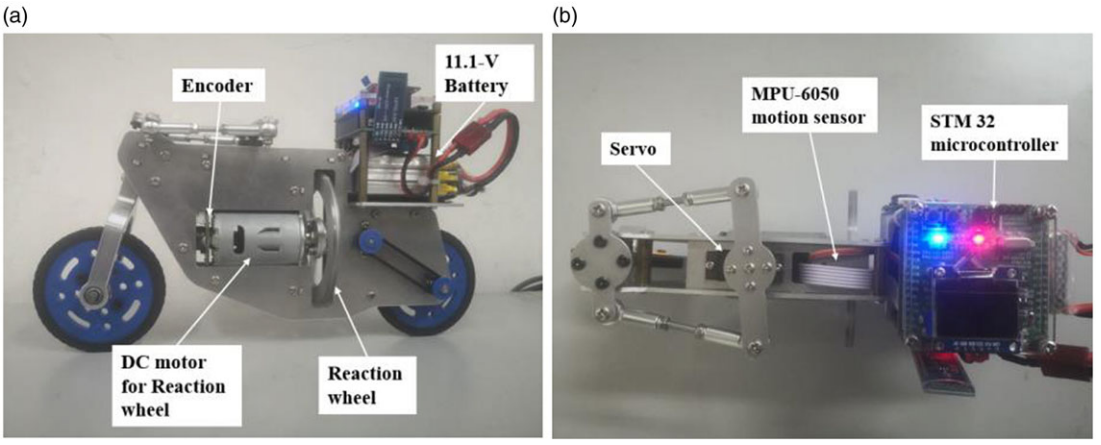


***Figure 5.*** *Experimental platform of UB. (a) Side view and (b) top view.*

## 4. Experimental verification

In this section, to demonstrate the superiority of the proposed controller, experiments compared with ITSM, AITSM and BFITSM controllers are carried out on a real UB system.

### *4.1. Experiment configurations*

The UB system used in the experiment is shown in Fig. 5, in which Fig. 5(a) and 5(b) are its side and top views, respectively. The UB system mainly consists of a body frame, two wheels, and a RW. The RW is installed at the centre of the bicycle body, and its rotational direction is the same as the bicycle's longitudinal direction. A servo motor is adopted to drive the RW with an equipped STM32 microcontroller. The UB is powered by an 11.1-volt lithium battery mounted at the rear bicycle. In addition, an encoder is used for measuring the speed of the RW, and an MPU-6050 motion sensor module is used to obtain the yaw angle of the bicycle.

The ITSM and AITSM controllers and the BFITSM controller in ref. [35] are used for comparison, presented as follows:

$$u_{ITSM} = N_0 v\dot{\delta} + P_0 v^2 \delta + M_0 \theta + J_0(\alpha_1 \dot{e} + \alpha_2 \dot{e}_I) + k_1 \text{sign}(s) \tag{53}$$

$$u_{AITSM} = N_0 v\dot{\delta} + P_0 v^2 \delta + M_0 \theta + J_0(\alpha_1 \dot{e} + \alpha_2 \dot{e}_I) + k_2 |s|^{\sigma} \text{ sign}(s) \tag{54}$$

$$u_{BFITSM} = N_0 v\dot{\delta} + P_0 v^2 \delta + M_0 \theta + J_0(\alpha_1 \dot{e} + \alpha_2 \dot{e}_I) + J_0 \hat{k} \text{sign}(s) \tag{55}$$

where the control parameters of above controller are chosen as the same as the proposed controller as given in Section 3.

### *4.2. Performance of stationary state (Case 1)*

Ideally, we hope that the roll angle of the UB maintains at 0° under control. However, in practice, due to the inertial action of the UB and the dead-zone characteristics of the motor, the roll angle of the UB cannot absolutely be maintained at 0°. Therefore, the control goal is to reduce the roll angle as much as possible. In this case, the UB system is keeping static. The experimental results are shown in Fig. 6.

Fig. 6(a) shows the roll angle of the UB under the action of four controllers. It can be seen that although the UB is kept within an acceptable range, the roll angle under the ITSM controller is the largest, which reaches 0.0084 rad. The proposed ELM-BFITSM controller can restrain the roll angle at

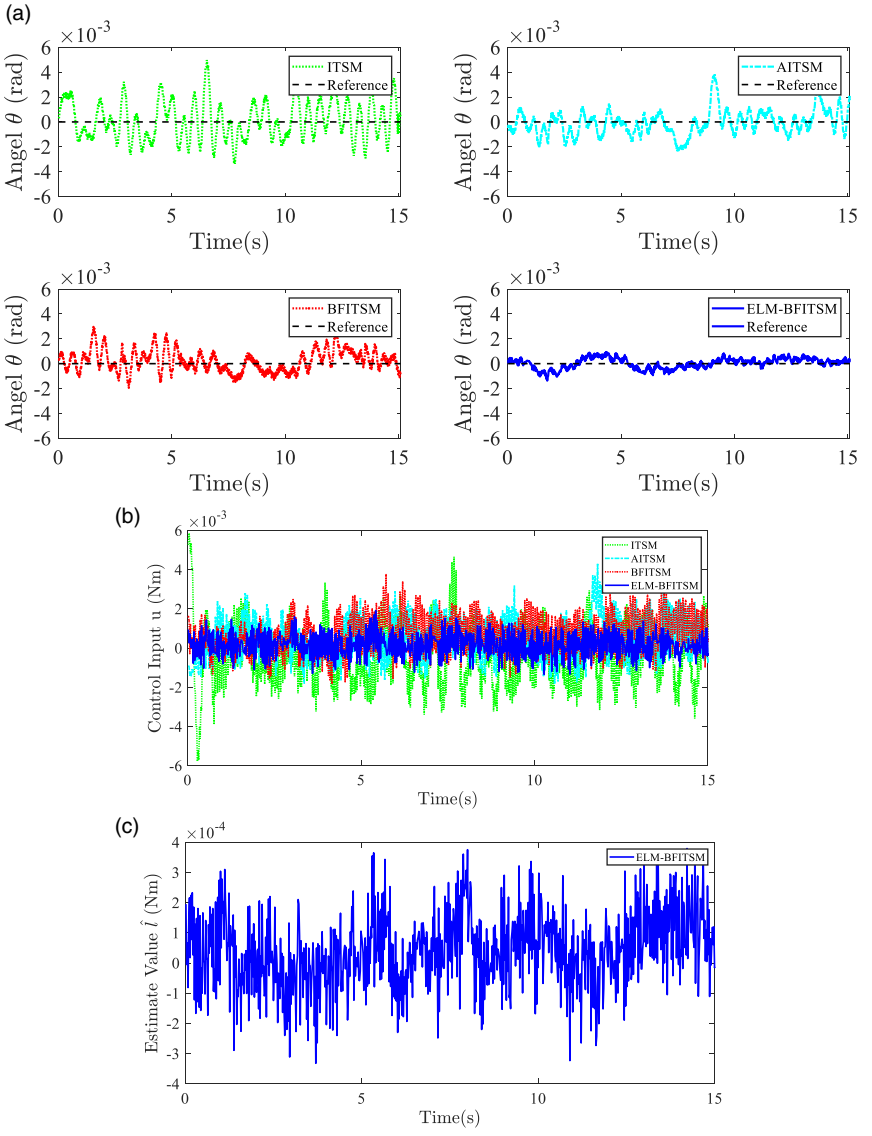


***Figure 6.*** *Control performance (Case 1). (a) Roll angle, (b) control input and (c) ELM.*

the smallest amplitude, and its maximum roll angle is only 0.0023 rad, which is smaller than AITSM control (0.0062 rad) and BFITSM control (0.0049 rad). Fig. 6(b) shows the control inputs of the four controllers. It can be seen that the chattering range of ELM-BFITSM control is 0.0033 Nm, which is significantly smaller than ITSM control (0.0116 Nm), AITSM control (0.0061 Nm) and BFITSM control (0.0055 Nm). The reason is that the ELM observer and BF-based adaptive algorithm can well compensate for effect of the lumped uncertainty on the closed-loop system.

Fig. 6(c) shows the lumped uncertainty estimation of the UB system. It can be seen that the estimated disturbance varies during the experiment. As shown in Fig. 6(a), the tracking error under ELM-BFITSM is ensured in the predefined bound of $\pm\frac{0.05}{2.4} = \pm 0.021$ rad, which implies the proposed ELM-BFITSM can exactly predefine the region of the roll angle tracking error.

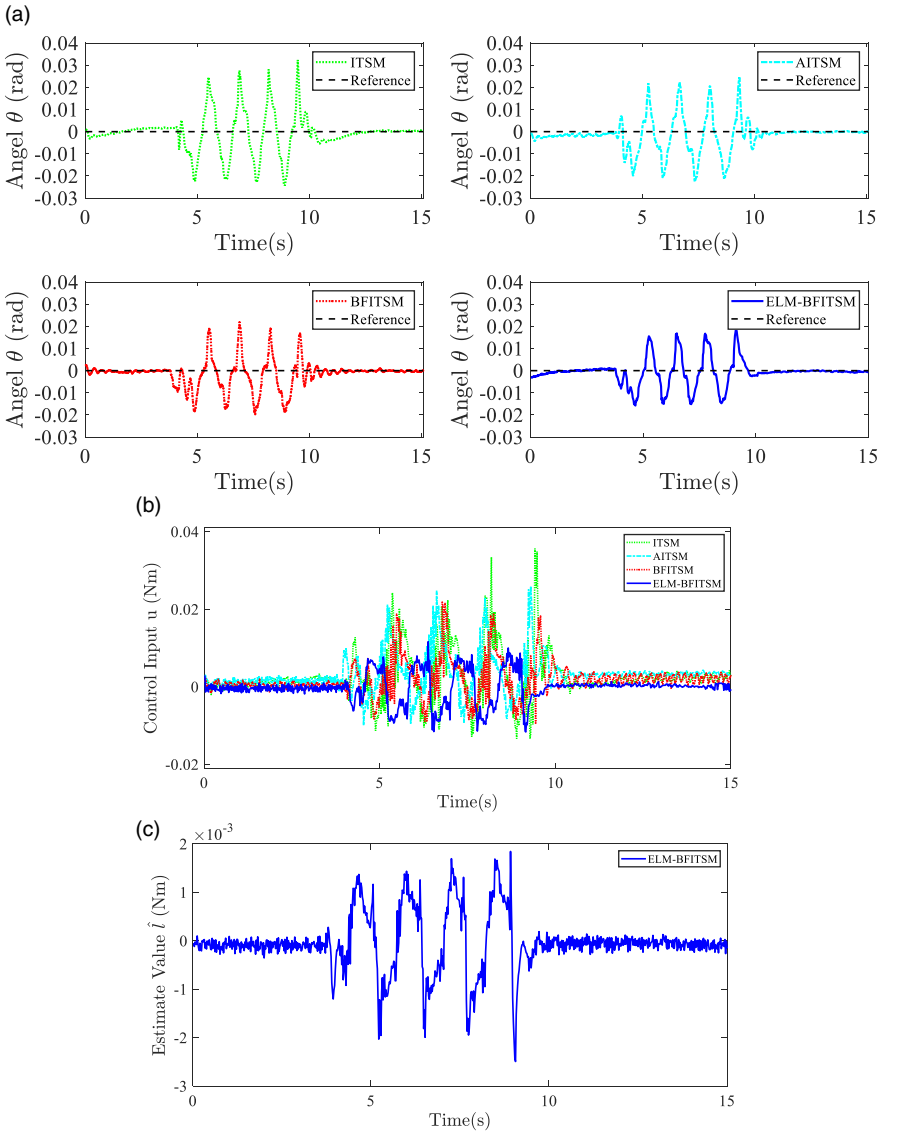


***Figure 7.*** *Control performance (Case 2). (a) Roll angle, (b) control input and (c) ELM estimated value.*

### *4.3. Performance of lateral force rejection (Case 2)*

To verify the robustness of the ELM-BFITSM against external disturbances, one-tenth of the motor power is used to generate a lateral force. The lateral force is suddenly applied to the UB when it is at a stationary balanced state. The experimental results are shown in Fig. 7. It can be observed that the ITSM control has the largest maximum roll angle reaching 0.057 rad. In addition, the BFITSM control achieves a smaller maximum roll angle (0.042 rad) than AITSM control (0.047 rad). Compared with the above three controllers, the performance of ELM-BFITSM controller is significantly improved, whose maximum roll angle is 0.034 rad. The control signals are shown in Fig. 7(b), while the disturbance estimation in the proposed control by ELM observer is depicted in Fig. 7(c). The proposed ELM observer does not require any training process and can adaptively adjusted the output weights such that the estimated results can be changed in real time with the disturbance. It can be seen that due to the effective compensation of the disturbance by using ELM observer, not only the smallest value of the control

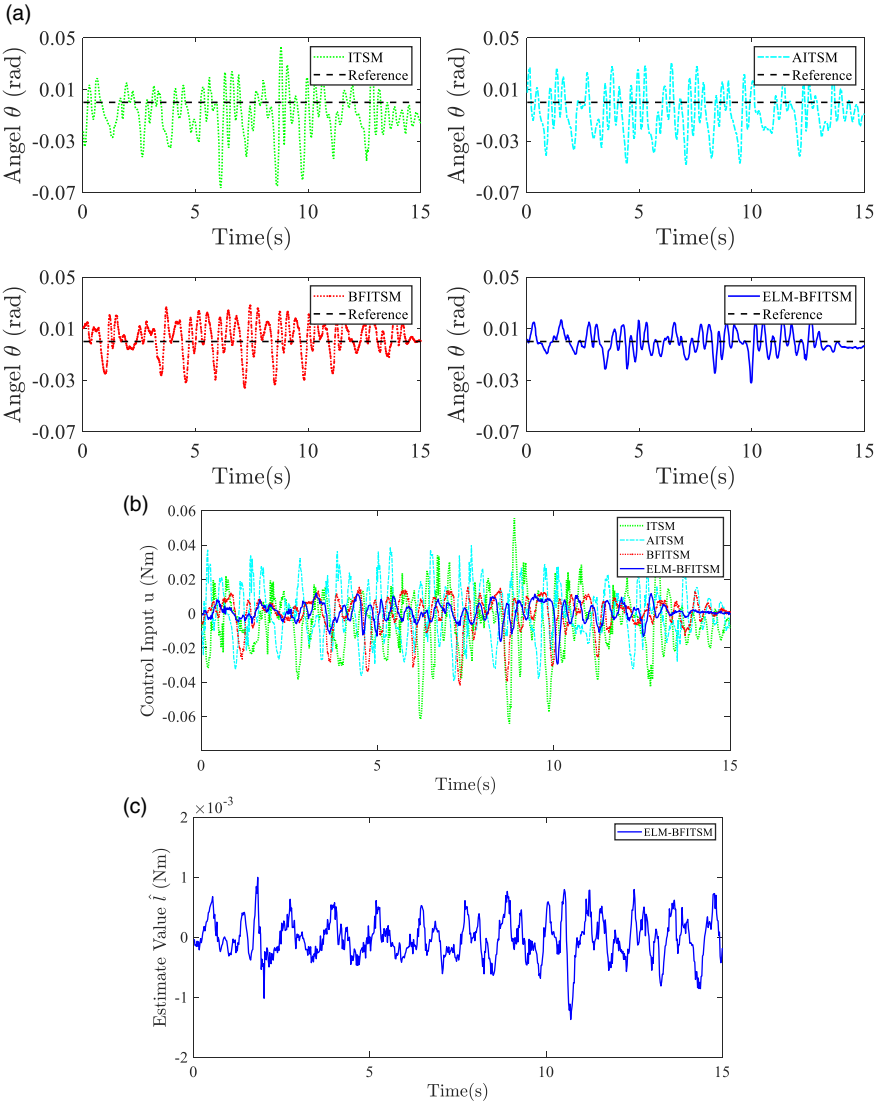


***Figure 8.*** *Control performance (Case 3). (a) Roll angle, (b) control input and (c) ELM estimated value.*

amplitude for the proposed control is achieved but also the best control performance of the proposed control is obtained as clearly shown in Fig. 7(a).

### *4.4. Performance of S-curve driving (Case 3)*

When the bicycle steers, the parametric uncertainty is activated due to the front wheel's motion. In order to further verify the strong robustness of the ELM-BFITSM controller, the UB system is required to follow an S-curve path in this case. The tracking performance of the controllers is shown in Fig. 8. It can be seen from Fig. 8(a) that ITSM has the worst control performance with a maximum roll angle reaching 0.11 rad. Due to the introduction of BF, the maximum roll angle of BFITSM control reduces to 0.064 rad, which is smaller than AITSM (0.079 rad). Moreover, the tracking error of ELM-BFITSM is 0.053 rad, which indicates that the ELM-BFITSM achieves the best control performance under the changing disturbance condition. As seen from Fig. 8(b), the control signal of ELM-BFITSM is smoother

***Table III.*** *Control performance comparisons.*

| | | RMSE (rad) | MAXE (rad) |
|---|---|---|---|
| Case 1 | ITSM | 0.00157 | 0.0084 |
| | AITSM | 0.00101 | 0.0062 |
| | BFITSM | 0.0009 | 0.0049 |
| | ELM-BFITSM | 0.00043 | 0.0023 |
| Case 2 | ITSM | 0.00844 | 0.057 |
| | AITSM | 0.00725 | 0.047 |
| | BFITSM | 0.00626 | 0.042 |
| | ELM-BFITSM | 0.005793 | 0.034 |
| Case 3 | ITSM | 0.01928 | 0.11 |
| | AITSM | 0.01812 | 0.079 |
| | BFITSM | 0.01312 | 0.064 |
| | ELM-BFITSM | 0.00853 | 0.053 |

than other three controllers, which does not have severe chattering problem. The estimate value of the uncertainty for the ELM-BFITSM control is shown in Fig. 8(c).

It can be seen from the above experimental results that, compared with ITSM, AITSM and BFITSM controllers, the proposed ELM-BFITSM control exhibits the best tracking performance. The reasons are given as follows: (i) Compared with the conventional ITSM control, better control performance is achieved due to the introduction of BF algorithm. (ii) Compared with adaptive ITSM and BFITSM control schemes, due to the fact that the ELM observer can compensate for the impacts of lumped uncertainty to effectively improve the control precision, the proposed control obtains the most superior control performance and robustness.

### *4.5. Performance comparisons*

For performance analysis, root mean square error (RMSE) and maximum error (MAXE) values of the sampled tracking error $e(i)$ are taken into consideration for comparisons, which are defined as

$$\mathrm{MAXE}(e) = \max(|e(i)|) \tag{56}$$

$$\mathrm{RMSE}(e) = \sqrt{\sum_{i=1}^{G} \frac{e^2(i)}{G}} \tag{57}$$

where $G$ is the number of the sampled tracking error. Table III and Figs. 9(a) and 9(b) show the performance comparisons of four controllers in three cases. It can be seen that the proposed controller achieves the smallest RMSE and MAXE values, while the ITSM controller behaves with the worst performance, followed by the AITSM and BFITSM controllers. It can be concluded that compared with the ITSM and adaptive ITSM controllers, the proposed ELM-BFITSM controller can achieve excellent control performance of the UB system in practical applications.

## 5. Conclusion

In this paper, an ELM-BFITSM controller has been developed for the balancing control of an UB system. It has been shown that the proposed control strategy comprises a BF-based adaptive ITSM for eliminating the reaching phase and an ELM observer for further compensating the lumped uncertainty. As a result, the disturbance can be estimated and be fed forward by the inherent ELM observer. Moreover, due to the BF-based adaptive law, the control gain is automatically updated according the disturbance

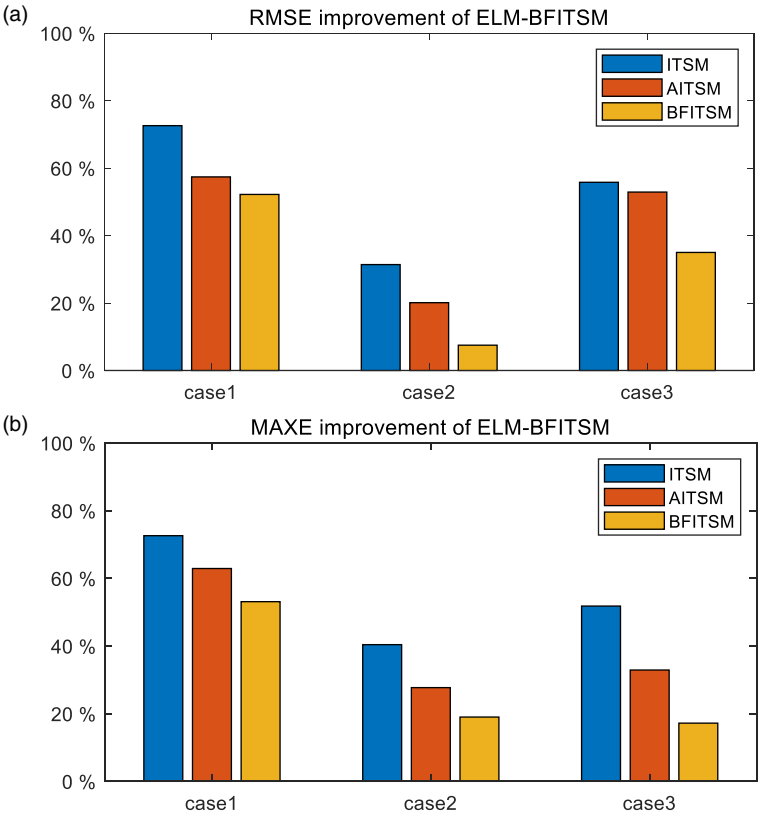


***Figure 9.*** *Control performance improvement of ELM-BFITSM.*

variations, and the overestimation is effectively suppressed. In addition, the proposed controller ensures that the roll angle of the UB converges to an exactly predefined region in finite time. The experimental results have verified the excellent control performance of the proposed controller compared to the conventional ITSM, conventional adaptive ITSM and BF-based ITSM controllers. Compared to ITSM, AITSM and BFITSM controllers, the RMSE of ELM-BFITSM control is improved by 72.6%, 57.4%, 52.2% in Case1; 31.4%, 20.1%, 7.5% in Case2 and 55.8%, 52.9%, 35% in Case3, respectively. In addition, the MAXE of the ELM-BFITSM control is improved by 72.6%, 62.9%, 53.1% in Case1; 40.4%, 27.7%, 19% in Case2 and 51.8%, 32.9%, 17.2% in Case3, respectively.

In practical applications, considering that some failures may occur such as actuator and sensor failures, our future research work will focus on sliding mode-based fault tolerant control of UB system.

**Author contributions.** Long Chen and Zhihui Jin conceived and designed the study. Guangyi Wang and Shuping He designed the hardware. Vladimir Stojanovic and Parisa Arabzadeh Bahri data gathering, simulation, and analyses. Zhihui Jin wrote this article. Ke Shao and Hai Wang provided guidance and supervision.

**Financial support.** This paper is partially supported by National Natural Science Foundation of China [Grant No. 61771178].

**Competing interests.** The authors declare no competing interest exist.

**Ethical approval.** None.

## References


[1] A. Shafiekhani, M. J. Mahjoob and M. Akraminia, "Design and implementation of an adaptive critic-based neuro-fuzzy controller on an unmanned bicycle," *Mechatronics* **28**, 115–123 (2015).

[2] L. Keo, S. Pornsarayouth, M. Yamakita and K. Ito, "Stabilization of an unmanned bicycle with flywheel balancer," *IFAC Proceed Vol* **43**(14), 475–480 (2010).

[3] B. Ahn, H. Kim, S. Lee and W. Ham, "Control of autonomous motion of unmanned electric bicycle," *IFAC Proceed Vol* **2**, 871–876 (2003).

[4] I. Park, J. Moon and W. Ham, "Control algorithm for stabilization of tilt angle of unmanned electric bicycle," *IFAC Proceed Vol* **34**(17), 165–170 (2001).

[5] U. Nenner, R. Linker and P.-O. Gutman, "Robust feedback stabilization of an unmanned motorcycle," *Control Eng Pract* **18**(8), 970–978 (2010).

[6] C.-K. Chen and T.-S. Dao, "Fuzzy control for equilibrium and roll-angle tracking of an unmanned bicycle," *Multibody Syst Dyn* **15**(4), 321–346 (2006).

[7] K. J. Astrom, R. E. Klein and A. Lennartsson, "Bicycle dynamics and control: Adapted bicycles for education and research," *IEEE Control Syst Mag* **25**(4), 26–47 (2005).

[8] M. Defoort and T. Murakami, "Sliding-mode control scheme for an intelligent bicycle," *IEEE Trans Ind Electron* **56**(9), 3357–3368 (2009).

[9] J. Xiong, N. Wang and C. Liu, "Stability analysis for the Whipple bicycle dynamics," *Multibody Syst Dyn* **48**, 311–335 (2020).

[10] M. A. Tofigh, M. J. Mahjoob, M. R. Hanachi and M. Ayati, "Fractional sliding mode control for an autonomous two-wheeled vehicle equipped with an innovative gyroscopic actuator," *Robot Auton Syst* **140**, 103756 (2021).

[11] S. Grau, S. Kapitola, S. Weiss and D. Noack, "Control of an over-actuated spacecraft using a combination of a fluid actuator and reaction wheels," *Acta Astronaut* **178**, 870–880 (2021).

[12] G. Buizza Avanzini, A. M. Zanchettin and P. Rocco, "Constrained model predictive control for mobile robotic manipulators," *Robotica* **36**(1), 19–38 (2018).

[13] N. Nfaileh, K. Alipour, B. Tarvirdizadeh and A. Hadi, "Formation control of multiple wheeled mobile robots based on model predictive control," *Robotica* **40**(9), 3178–3213 (2022).

[14] F. Dimeas, D. V. Sako, V. C. Moulianitis and N. A. Aspragathos, "Design and fuzzy control of a robotic gripper for efficient strawberry harvesting," *Robotica* **33**(5), 1085–1098 (2015).

[15] F. Li, Z. Zhang, Y. Wu, Y. Chen, K. Liu and J. Yao, "Improved fuzzy sliding mode control in flexible manipulator actuated by PMAs," *Robotica* **40**(8), 2683–2696 (2022).

[16] J. A. Chocoteco, R. Morales, V. Feliu and H. Sira-Ramírez, "Robust output feedback control for the trajectory tracking of robotic wheelchairs," *Robotica* **33**(1), 41–59 (2015).

[17] F. Pierri, G. Muscio and F. Caccavale, "An adaptive hierarchical control for aerial manipulators," *Robotica* **36**(10), 1527–1550 (2018).

[18] E. Sariyildiz, R. Mutlu and H. Yu, "A sliding mode force and position controller synthesis for series elastic actuators," *Robotica* **38**(1), 15–28 (2020).

[19] M. R. Islam, M. Rahmani and M. H. Rahman, "A novel exoskeleton with fractional sliding mode control for upper limb rehabilitation," *Robotica* **38**(11), 2099–2120 (2020).

[20] A. Villanueva, L. F. Luque-Vega, L. E. González-Jiménez and C. A. Arellano-Muro, "Robust multimode flight framework based on sliding mode control for a rotary UAV," *Robotica* **39**(4), 699–717 (2021).

[21] S. Liu, G. Liu and S. Wu, "Adaptive sliding tracking control for nonlinear uncertain robotic systems with unknown actuator nonlinearities," *Robotica* **40**(8), 2527–2546 (2022).

[22] L. Qiao and W. Zhang, "Adaptive non-singular integral terminal sliding mode tracking control for autonomous underwater vehicles," *IET Control Theory Appl* **11**(8), 1293–1306 (2017).

[23] L. Qiao and W. Zhang, "Trajectory tracking control of AUVs via adaptive fast nonsingular integral terminal sliding mode control," *IEEE Trans Industr Inform* **16**(2), 1248–1258 (2020).

[24] C.-K. Lin, "Nonsingular terminal sliding mode control of robot manipulators using fuzzy wavelet networks," *IEEE Trans Fuzzy Syst* **14**(6), 849–859 (2006).

[25] H. Ma, W. Liu, Z. Xiong, Y. Li, Z. Liu and Y. Sun, "Predefined-time barrier function adaptive sliding-mode control and its application to piezoelectric actuators," *IEEE Trans Industr Inform* **18**(12), 8682–8691 (2022).

[26] C. H. Chiu and C. Y. Wu, "Bicycle robot balance control based on a robust intelligent controller," *IEEE Access* **8**, 84837–84849 (2020).

[27] C-L. Hwang, H-M. Wu and C-L. Shih, "Fuzzy sliding-mode underactuated control for autonomous dynamic balance of an electrical bicycle," *IEEE Trans Control Syst Technol* **17**(3), 658–670 (2009).

[28] Z. Yao, F. Xu, G.-P. Jiang and J. Yao, "Data-driven control of hydraulic manipulators by reinforcement learning," *IEEE/ASME Trans Mechatro* (2023).

[29] L. Chen, B. Yan, H. Wang, K. Shao, E. Kurniawan and G. Wang, "Extreme-learning-machine-based robust integral terminal sliding mode control of bicycle robot," *Control Eng Pract* **121**, 105064 (2022).

[30] Y. H. Hu and H. Wang, "Robust tracking control for vehicle electronic throttle using adaptive dynamic sliding mode and extended state observer," *Mech Syst Signal Process* **135**, 106375 (2020).

[31] L. Chen, J. Liu, H. Wang, Y. Hu, X. Zheng, M. Ye and J. Zhang, "Robust control of reaction wheel bicycle robot via adaptive integral terminal sliding mode," *Nonlinear Dyn* **104**(3), 2291–2302 (2021).

[32] M. Ye and H. Wang, "Robust adaptive integral terminal sliding mode control for steer-by-wire systems based on extreme learning machine," *Comput Electr Eng* **86**, 106756 (2020).
[33] Y. Feng, X. Yu and Z. Man, "Non-singular terminal sliding mode control of rigid manipulators," *Automatica* **38**(12), 2159–2167 (2002).
[34] K. Shao, J. Zheng, H. Wang, X. Wang, R. Lu and Z. H. Man, "Tracking control of a linear motor positioner based on barrier function adaptive sliding mode," *IEEE Trans Industr Inform* **17**(11), 7479–7488 (2021).
[35] M. Labbadi, H. A. Hashim, A. E. E. Eltoukhy and M. Djemai, "Barrier Function-Based Adaptive Nonsingular Fast Terminal Sliding Mode Control for Disturbed UAVs," In: *2022 European Control Conference (ECC). IEEE*, (2022) pp. 975–980.
[36] G.-B. Huang, Q.-Y. Zhu and C.-K. Siew, "Extreme learning machine: Theory and applications," *Neurocomputing* **70**(1-3), 489–501 (2006).
[37] F. Huang, J. Lu, J. Tao, L. Li, X. Tan and P. Liu, "Research on optimization methods of elm classification algorithm for hyperspectral remote sensing images," *IEEE Access* **7**, 108070–108089 (2019).
[38] K. Yan, Z. Ji, H. Lu, J. Huang, W. Shen and Y. Xue, "Fast and accurate classification of time series data using extended ELM: Application in fault diagnosis of air handling units," *IEEE Trans Syst Man Cybern: Syst* **49**(7), 1349–1356 (2019).
[39] K. Shao, J. Zheng, K. Huang, H. Wang, Z. Man and M. Fu, "Finite-time control of a linear motor positioner using adaptive recursive terminal sliding mode," *IEEE Trans Ind Electron* **67**(8), 6659–6668 (2020).
[40] E. Moulay and W. Perruquetti, "Finite time stability and stabilization of a class of continuous systems," *J Math Anal Appl* **323**(2), 1430–1443 (2006).

## Appendix A

In this paper, the control law is designed as

$$u = u_0 + u_1 + u_2 \tag{58}$$

Then, we have

$$\begin{aligned} |u| &< |u_0| + |u_1| + |u_2| \\ &< \left|N_0 v\dot{\delta} + P_0 v^2\delta + M_0\theta + J_0(\alpha_1\dot{e} + \alpha_2\dot{e}_I)\right| + \left|\hat{l}\right| + \left|J_0\hat{k}sign(s)\right| \\ &< \left|N_0 v\dot{\delta} + P_0 v^2\delta + M_0\theta + J_0\left(\alpha_1\dot{\theta} + \alpha_2 e^{\frac{q1}{q2}}\right)\right| + \left|\hat{l}\right| + \left|J_0\hat{k}\right| \\ &< \left|N_0 v\dot{\delta} + P_0 v^2\delta\right| + \left|\hat{l}\right| + \left|J_0\hat{k}\right| + \left|M_0\theta + J_0\alpha_2\theta^{q1/q2}\right| + \left|J_0\alpha_1\dot{\theta}\right| \\ &< \left|N_0 v\dot{\delta} + P_0 v^2\delta\right| + \left|\hat{l}\right| + \left|J_0\hat{k}\right| + max(M_0, J_0\alpha_2)\,|\theta| + J_0\alpha_1\left|\dot{\theta}\right| \end{aligned} \tag{59}$$

where $v$ is the forward speed of the UB, $\delta$ is the steering angle of the front wheel relative to the positive direction of UB, which are set as the small value and change continuously in the experiment. $\hat{l}$ is the estimated result of ELM observer, which is bounded. $\hat{k}$ is the proposed adaptive law. If $\hat{k} = \mu\int_0^t \exp(\sigma|s|)|s|d\tau$, the $\hat{k}$ is bounded because of the finite-time accessibility. If $\hat{k} = f_b(s)$, the $\hat{k}$ is bounded because the $\hat{k}$ will increase quickly to pull $|s|$ back when $|s|$ gradually increases, so that the $\hat{k}$ is a large but bounded value.

Therefore, when $\zeta_0 > |N_0 v\dot{\delta} + P_0 v^2\delta| + |\hat{l}| + |J_0\hat{k}|$, $\zeta_1 = max(M_0, J_0\alpha_2)$ and $\zeta_2 = J_0\alpha_1$, the following inequality holds:

$$|u| < \zeta_0 + \zeta_1\,|\theta| + \zeta_2|\dot{\theta}| \tag{60}$$

## Appendix B

Based on (7), the $\ddot{\theta}$ is expressed as

$$\ddot{\theta} = \frac{N_0 v\dot{\delta}}{J_0} + \frac{P_0 v^2\delta}{J_0} + \frac{M_0\theta}{J_0} + \frac{1}{J_0}(l - u) \tag{61}$$

The lumped uncertainty $l$ is given by

$$l = d + \Delta N v\dot{\delta} + \Delta P v^2\delta + \Delta M\theta - \Delta J\ddot{\theta} \tag{62}$$

Then, we obtain:

$$l = d + \Delta N v\dot{\delta} + \Delta P v^2\delta + \Delta M\theta - \Delta J\left(\frac{N_0 v\dot{\delta}}{J_0} + \frac{P_0 v^2\delta}{J_0} + \frac{M_0\theta}{J_0} + \frac{1}{J_0}(l-u)\right) \tag{63}$$

Rearranging the terms, we get:

$$\begin{aligned} l &= \frac{\Delta J}{J_0\left(1+\frac{\Delta J}{J_0}\right)}u + \frac{d + \Delta N v\dot{\delta} + \Delta P v^2\delta}{\left(1+\frac{\Delta J}{J_0}\right)} + \frac{\Delta M\theta}{\left(1+\frac{\Delta J}{J_0}\right)} - \frac{\Delta J M_0\theta}{J_0\left(1+\frac{\Delta J}{J_0}\right)} - \frac{\Delta J N_0 v\dot{\delta} + \Delta J P_0 v^2\delta}{J_0\left(1+\frac{\Delta J}{J_0}\right)} \\ &= \frac{\Delta J}{J_0+\Delta J}u + \frac{(J_0-\Delta J)\,\Delta M\theta}{J_0+\Delta J} + \frac{J_0(d+\Delta N v\dot{\delta} + \Delta P v^2\delta)}{J_0+\Delta J} - \frac{\Delta J N_0 v\dot{\delta} + \Delta J P_0 v^2\delta}{J_0+\Delta J}\Bigg) \end{aligned} \tag{64}$$

Therefore, we have

$$|l| \le \left|\frac{\Delta J}{J_0+\Delta J}\right||u| + \left|\frac{(J_0-\Delta J)\,\Delta M}{J_0+\Delta J}\right||\theta| + \left|\frac{J_0\left(\left|d+\Delta N v\dot{\delta}+\Delta P v^2\delta\right|\right)}{J_0+\Delta J}\right| + \left|\frac{\Delta J(N_0 v\dot{\delta}+P_0 v^2\delta)}{J_0+\Delta J}\right| \tag{65}$$

In this work, the disturbance $d$ and the uncertain items $\Delta N$, $\Delta P$, $\Delta M$ and $\Delta J$ are considered to be bounded. In addition, the steering angle $\delta$ is continuously changed such that its derivative is bounded as well [29]. Therefore, the following inequalities for the bounded property are given as

$$|d| < D, \left|\Delta N v\dot{\delta}\right| < \partial_1, \left|\Delta P v^2\delta\right| < \partial_2 \tag{66}$$

$$D + \partial_1 + \partial_2 < \partial_3 \tag{67}$$

$$\left|\frac{J_0\left(|d| + \left|\Delta N v\dot{\delta}\right| + \left|\Delta P v^2\delta\right|\right)}{J_0+\Delta J}\right| + \left|\frac{\Delta J(N_0 v\dot{\delta}+P_0 v^2\delta)}{J_0+\Delta J}\right| < \left|\frac{J_0\partial_3}{J_0+\Delta J}\right| + \left|\frac{\Delta J(N_0 v\dot{\delta}+P_0 v^2\delta)}{J_0+\Delta J}\right| < \beta_0 \tag{68}$$

$$\left|\frac{\Delta J}{J_0+\Delta J}\right| < \beta_1 \tag{69}$$

$$\left|\frac{(J_0-\Delta J)\,\Delta M}{J_0+\Delta J}\right| < \beta_2 \tag{70}$$

Then, we yield:

$$|l| \le \beta_0 + \beta_1|u| + \beta_2|\theta|$$

As can be seen that the upper bound of the lumped uncertainty $l$ is associated with the structure of the designed controller. From (9), we have

$$|l| \le \beta_0 + \beta_1\left(\zeta_0 + \zeta_1|\theta| + \zeta_2|\dot{\theta}|\right) + \beta_2|\theta| = \beta_0 + \beta_1\zeta_0 + \beta_1\zeta_1|\theta| + \beta_2|\theta| + \beta_1\zeta_2|\dot{\theta}| \tag{71}$$

Thus, we obtain the expression:

$$|l| < \bar{l} = \mu_0 + \mu_1|\theta| + \mu_2|\dot{\theta}| \tag{72}$$

where:

$$\mu_0 = \beta_0 + \beta_1\zeta_0 \tag{73}$$

$$\mu_1 = \beta_1\zeta_1 + \beta_2 \tag{74}$$

$$\mu_2 = \beta_1\zeta_2 \tag{75}$$

This completes the proof.

## Appendix C

Suppose a first-order non-linear differential inequality given by

$$\dot{V} + \kappa V^{\eta} \leq 0 \tag{76}$$

where $\kappa > 0$, $0 < \eta < 1$. $V(x)$ is a positive Lyapunov function with respect to the state $x \in R$. Then, the function $V(x)$ will converge from any given initial condition $V(x(0)) = V(0)$ to the origin in the finite time given by

$$t_r \leq \frac{\mathrm{V}^{1-\eta}(0)}{\kappa(1-\eta)} \tag{77}$$

The details can refer to ref. [40] and references therein.

## Appendix D

The sliding function (14)-(15) can be rewritten as

$$\dot{e} + \left(\alpha_1 - \frac{s}{e}\right) e + \alpha_2 \int_0^t e^{q_1/q_2} = 0 \tag{78}$$

Since $|s| \leq \varepsilon$, if $|e| > \frac{\varepsilon}{\alpha_1}$, we have $\alpha_1 - \frac{\varepsilon}{e} := \alpha_1' > 0$. It is clear that $e$ is decreasing to zero in finite time according to (78) [18]. In other words, $e$ will be bounded by

$$|e| \leq \frac{\varepsilon}{\alpha_1} \tag{79}$$

in finite time.

**Cite this article:** L. Chen, Z. Jin, K. Shao, G. Wang, S. He, V. Stojanovic, P. A. Bahri and H. Wang (2024). "Adaptive integral terminal sliding mode control of unmanned bicycle via ELM and barrier function", Robotica **42**, 2635–2657. https://doi.org/10.1017/S0263574724000997